ACS Infectious Diseases

pubs.acs.org/journal/aidcbc

Article

Erythro-PmBs: A Selective Polymyxin B Delivery System Using Antibody-Conjugated Hybrid Erythrocyte Liposomes

Hannah Krivić, Sebastian Himbert, Ruthie Sun, Michal Feigis, and Maikel C. Rheinstädter*

Cite This: *ACS Infect. Dis.* 2022, 8, 2059−2072

Read Online

ACCESS | Metrics & More | Article Recommendations

ABSTRACT: As a result of the growing worldwide antibiotic resistance crisis, many currently existing antibiotics have become ineffective due to bacteria developing resistive mechanisms. There are a limited number of potent antibiotics that are successful at suppressing microbial growth, such as polymyxin B (PmB); however, these are often deemed as a last resort due to their toxicity. We present a novel PmB delivery system constructed by conjugating hybrid erythrocyte liposomes with antibacterial antibodies to combine a high loading efficiency with guided delivery. The retention of PmB is enhanced by incorporating negatively charged lipids into the red blood cells' cytoplasmic membrane (RBC_{cm}). Anti-*Escherichia coli* antibodies are attached to these hybrid erythrocyte liposomes by the inclusion of DSPE-PEG maleimide linkers. We show that these erythro-PmBs have a loading efficiency of ∼90% and are effective in delivering PmB to *E. coli*, with values for the minimum inhibitory concentration (MIC) being comparable to those of free PmB. The MIC values for *Klebsiella aerogenes*, however, significantly increased well beyond the resistant breakpoint, indicating that the inclusion of the anti-*E. coli* antibodies enables the erythro-PmBs to selectively deliver antibiotics to specific targets.

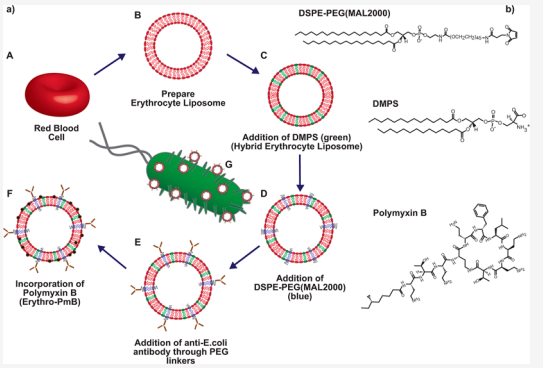

KEYWORDS: *erythrocyte liposomes, antibiotics, targeted drug delivery, polymyxin B encapsulation and delivery, antibody anchoring, antibiotic specificity*

The emergence of the antibiotic resistance crisis is the product of antibiotic overuse in medical and industrial settings.[1−5] As a result, this has led to selection pressures on bacteria, leading to the development and rapid spread of resistant mutations.[2] Without immediate global intervention and management, bacteria can evolve to develop multidrug resistance (MDR), where infections once curable by common antibiotics become difficult to treat.[6] Such management steps may include improved diagnostic techniques, controlled antibiotic prescription, and the development of novel antimicrobial agents.[2−4,7] Enterobacteriaceae bacteria, such as *Escherichia coli* and *Klebsiella* species, are responsible for many serious infections: pneumonia, gastroenteritis, and bloodstream infections.[6] Enterobacteriaceae are also the major players in MDR and are thus a target species for the development of novel antimicrobial agents.[6]

Polymyxin B (PmB) has emerged as a promising treatment against resistant bacteria due to its high bactericidal activity.[8−10] PmB is a cyclic cationic peptide that interacts with the lipopolysaccharides (LPSs) in the outer membrane of Gram-negative bacteria through their lipid A component, leading to increased membrane permeability and bacterial death.[8,11] Despite being highly potent, PmB is reserved as a last-resort treatment due to toxic side effects such as nephrotoxicity, neurotoxicity, and neuromuscular blockade.[8] Nephrotoxicity, in particular, is the most detrimental side effect in which increasing concentrations of PmB treatment can induce apoptosis in kidney proximal tubular cells.[12,13] In order to successfully treat infections from resistant bacteria, higher-dose treatments are often administered, increasing the likelihood of nephrotoxicity.[14] Optimization of PmB delivery is required to effectively minimize toxicity with high efficacy.[9,15,16]

The use of carriers for antibiotic delivery has been of recent interest to improve drug stability, targeted delivery, and uniform distribution in the target organ to reduce side effects and to improve success against resistant strains of bacteria.[14,15,17] Nanoparticles have shown promise as drug carriers as antibiotics can be conjugated to their surface or encapsulated inside. Additionally, nanoparticles have the potential to deliver lower doses than free antibiotics while effectively treating bacterial infections. Examples of nano-

Received: January 10, 2022
Published: September 29, 2022

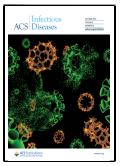

https://doi.org/10.1021/acsinfecdis.2c00017
ACS Infect. Dis. 2022, 8, 2059−2072

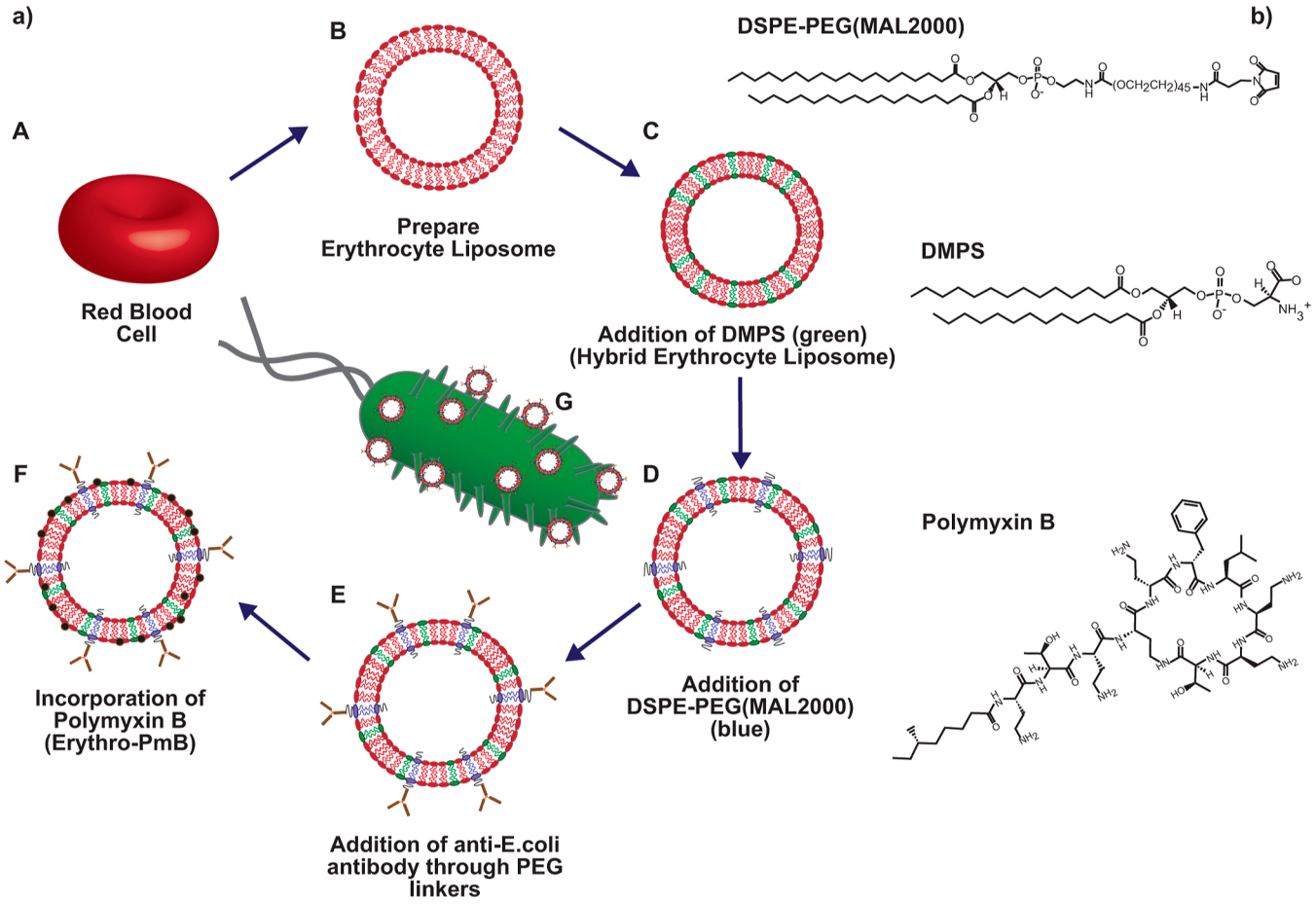

Figure 1. (a) Schematic of the preparation protocol. Erythrocyte liposomes are prepared from human red blood cells (A,B) and are modified through the addition of negatively charged DMPS (C) to enhance polymyxin B (PmB) retention. Anti-*E. coli* antibodies were conjugated to PEG-MAL(2000) to achieve specificity (D,E). The resulting hybrid erythrocyte liposome is mixed with PmB to produce the erythro-PmBs (D). (b) Schematics of the molecules used in this study: 1,2-distearoyl-*sn*-glycero-3-phosphoethanolamine-*N*-[maleimide(polyethylene glycol)-2000] (PEG-MAL(2000)), 1,2-dimyristoyl-*sn*-glycero-3-phospho-L-serine (DMPS), and PmB ($C_{56}H_{100}N_{16}O_{17}S$).

particles include polymer-based nanoparticles, metallic nanoparticles, and liposomes.[18−22]

Liposomes have been successfully used as delivery systems for antibiotics. Liposomes can fuse with the bacterial membrane, allowing for the delivery of high antibiotic concentrations. Electrostatic interactions may play an important role in this process as biofilm formation was reduced when positively charged clarithromycin was encapsulated in negatively charged liposomes. However, positive liposome formulations required smaller clarithromycin dosages, reducing toxicity.[23] Liposomes are typically composed of phospholipids that form one or more bilayers, and their size, composition, charge, pH, and fluidity can be modified. One of the advantages of liposomal drug delivery is sustained release: the antibiotic can be retained in the liposome for long periods in circulation, allowing greater doses to be administered to the target. The surface of the liposomes can be modified to include proteins and ligands targeting different tissues and organs. Known limitations of liposomal drug delivery are chemical instability during storage, physical instability under physiological conditions that potentially lead to drug leakage, and low encapsulation efficiencies.[24]

Red blood cells (RBCs) have been investigated as drug carriers as they have high biocompatibility and can prolong the life of drugs in circulation for weeks.[25] The challenge with modifying RBCs is that they may be taken up by macrophages in the spleen and liver, where they undergo lysosomal degradation. The conjugation of drugs to the RBC surface has shown promise as it reduces damage, retains high RBC biocompatibility, and enhances pharmacokinetics. RBCs were found to effectively deliver drugs to intravascular targets and targets in the reticuloendothelial system. However, delivery of RBCs to other tissues is limited due to inaccessibility.[26,27] For instance, it has been shown that thrombomodulin (TM) conjugated to RBCs can effectively inhibit clot formation with improved pharmacodynamics and bioavailability compared to free TM.[28] Many therapeutic proteins are limited by the humoral immune response and are thus not used in clinical settings. However, by binding to erythrocytes, the immunological tolerance to *Escherichia coli*L-asparaginase-II (ASNase) was increased,[29] indicating that enzyme conjugation to erythrocytes can enhance pharmacodynamics. RBCs' blood groups serve as protection from the body's immune system, making the addition of molecules such as polyethylene glycol (PEG) unnecessary to increase the drug carrier lifetime in circulation.[26] Even with the addition of PEG, synthetic liposomes only exhibit a half-life in blood of 3−6 h, significantly less than the RBC half-life of 10−15 days. The conjugation of synthetic nanoparticles to RBCs has been explored as a strategy to increase their survival in circulation.[27]

https://doi.org/10.1021/acsinfecdis.2c00017
ACS Infect. Dis. 2022, 8, 2059−2072

Their increased survival in circulation and enhanced pharmacodynamics make RBCs a promising platform for targeted delivery of PmB.

Here, we present a novel PmB delivery system by conjugating hybrid erythrocyte liposomes with antibacterial antibodies to combine a high loading efficiency with guided delivery. As pictured in Figure 1a, erythrocyte liposomes are prepared from human RBCs. PmB encapsulation is enhanced by incorporating negatively charged 1,2-dimyristoyl-*sn*-glycero-3-phospho-L-serine (DMPS) into the RBC_{cm}. Anti-*E. coli* antibodies are attached to these hybrid erythrocyte liposomes by the inclusion of 1,2-distearoyl-*sn*-glycero-3-phosphoethanolamine-*N*-[maleimide(polyethylene glycol)-2000] (PEG-MAL(2000)) linkers prior to PmB encapsulation (all molecules are shown in Figure 1b). We show that these erythro-PmBs have a high loading efficiency of ~90% and are effective at delivering PmB to *E. coli*, with the minimum inhibitory concentration (MIC) values comparable to those of free PmB (MIC^f). MIC^E values for *Klebsiella aerogenes*, however, significantly increased well beyond the concentration at which the bacteria become susceptible—the resistant breakpoint—to PmB, indicating that inclusion of the anti-*E. coli* antibodies to erythro-PmBs enables antibiotic delivery to specific targets with high selectivity.

RESULTS

Antibiotic Retention Is Maximized by Optimizing the Composition of Hybrid Erythrocyte Liposomes. Initially, the retention of PmB in hybrid erythrocyte liposomes was optimized by varying the fraction of negatively charged DMPS to the RBC_{cm} lipids and varying the ratio of PmB to the hybrid erythrocyte liposome. The inclusion of DMPS was based on the assumption that electrostatic interactions play a role in the interaction between antibiotics and liposomes[10] and that retention of the cationic PmB can be increased by adding negative charges to the erythrocyte liposomes. Growth curves for *E. coli* were measured for the following formulations: (1) 5 mol % DMPS and 1000 PmB per erythrocyte liposome, (2) 5 mol % DMPS and 10000 PmB per erythrocyte liposome, (3) 10 mol % DMPS and 1000 PmB per erythrocyte liposome, and (4) 10 mol % DMPS and 10000 PmB per erythrocyte liposome, as shown in Figure 2. The efficiency was quantified by the relative duration of the lag phase: the shorter the lag phase (the closer the curve mimics an undisturbed growth curve), the higher the retention of PmB in the erythrocyte liposome. This method is based on the premise that erythrocyte liposomes lacking the corresponding antibacterial antibodies will not interact with bacteria and therefore should not deliver PmB, as will be shown further below. Hybrid erythrocyte liposomes consisting of 5 mol % DMPS and loaded with 1000 PmB per liposome showed the highest retention and were thus selected for further investigations.

Molecular dynamics (MD) simulations of hybrid erythrocyte liposomes with 5 and 10 mol % DMPS exposed to 2 mol % PmB were run for 200 ns, each, to elucidate the molecular mechanism behind these experimental findings. The number of lipid molecules in a hybrid erythrocyte liposomes was estimated to ~50 000.[42] Two mol % PmB thus correspond in about 1000 PmB molecules per liposome, in agreement with the experimental conditions. A resulting snapshot of a hybrid erythrocyte membrane containing 5 mol % DMPS treated with 2 mol % PmB is shown in Figure 3a. The phosphate head groups of all membrane lipids are highlighted in orange, the

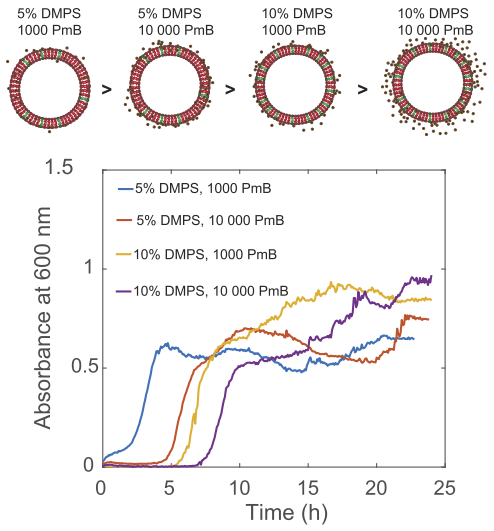

Figure 2. Retention of PmB in hybrid erythrocyte liposomes for varying fractions of DMPS and ratios of PmB to erythrocyte liposome was optimized by measuring growth curves for *E. coli*. Shown is absorbance at 600 nm (OD600) over a 24 h period at a PmB concentration of 0.32 μg/mL (0.5 MIC^f). Hybrid erythrocyte liposomes consisting of 5 mol % DMPS and a ratio of 1000 PmB per liposome resulted in the highest PmB retention, as indicated by the shortest lag phase.

polyunsaturated fatty acids (PUFAs) and DMPS are highlighted in purple and green, and the remaining membrane lipids are highlighted in silver. In the pure erythrocyte membranes in Figure 3b, PmB molecules were found to spontaneously attach to the membrane within a few nanoseconds and form clusters on the membrane. PmB was found to preferably localize in regions of high PUFA density. Some PmBs were found to insert their hydrophobic acyl tail in between the lipid head groups of the PUFA clusters, as shown in Figure 3c.

When increasing the negative membrane charge by incorporating 5 mol % DMPS in Figure 3d, PmB spontaneously made contact with the membranes and localized predominantly to PUFA-rich areas of the erythrocyte membranes. A larger fraction of the molecules inserted their acyl tail end into the hydrophobic membrane core with an angle almost parallel to the membrane normal. In addition, the PmB molecules are positioned deeper into the lipid head group region as compared to the pure erythrocyte membranes. When the anionic DMPS fraction was further increased to 10 mol % in Figure 3f, acyl tail insertion was shown to reduce with the PmB adhering more to the membrane surface in Figure 3g.

MD simulations were also run to investigate the maximum PmB loading of the liposomes in the experiments. To understand what happens when liposomes are exposed to high PmB concentrations, Figure 4 shows snapshots of MD simulations at 200 ns of erythrocyte membranes consisting of 5 mol % DMPS that were exposed to 20 mol % PmB (corresponding to ~10 000 PmB molecules per erythrocyte liposome). PmB molecules are shown to aggregate and adhere to the membrane surface in Figure 3a. The acyl tails of PmB appear to insert in between the lipid heads in both regions of high and low PUFA density, as shown in Figure 3b. However, not all PmB molecules have adhered or inserted into the membrane, in contrast to membranes exposed to 2 mol % PmB as the accessible membrane area is limited.

https://doi.org/10.1021/acsinfecdis.2c00017
ACS Infect. Dis. 2022, 8, 2059−2072

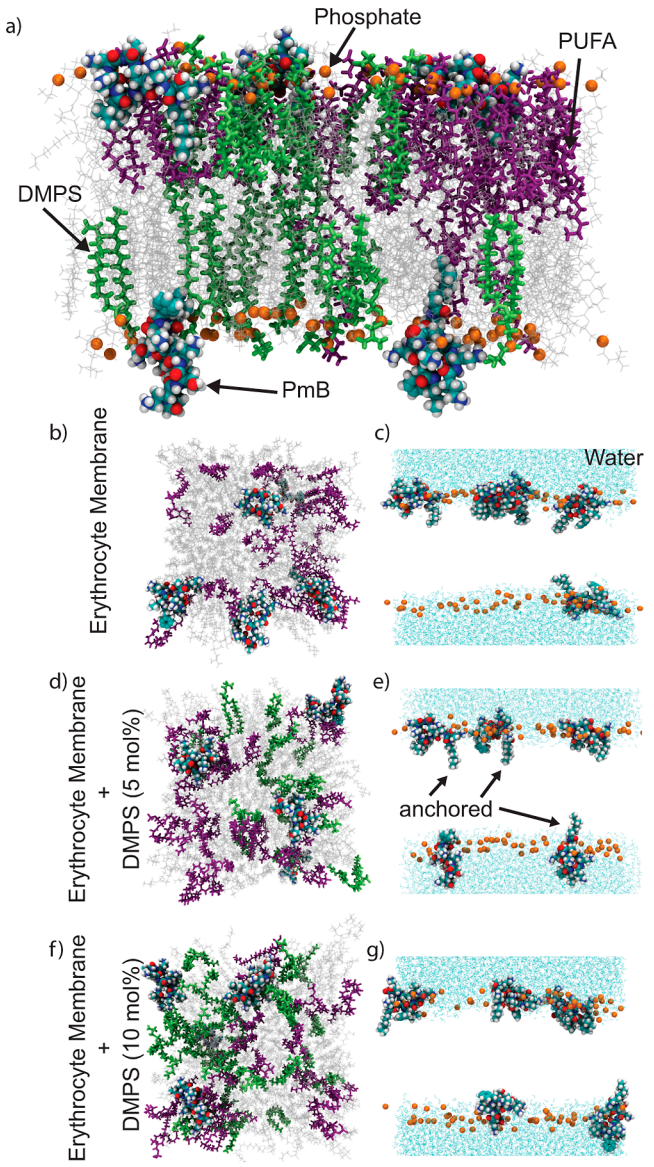

Figure 3. (a) Snapshot of MD simulation at 200 ns of hybrid erythrocyte membranes containing 5 mol % DMPS treated with 2 mol % PmB. Highlighted are the phosphate groups (orange), PUFAs (purple), DMPS (green), and remaining membrane lipids (silver). Top-view snapshots of erythrocyte membranes treated with 2 mol % PmB with (b) no PmB, (d) 5, and (f) 10 mol % DMPS. Side-view snapshots reveal PmB membrane interaction with erythrocyte membranes containing (c) no DMPS, (e) 5, and (g) 10 mol % DMPS. All membrane lipids were hidden, and the surrounding water molecules are highlighted in blue.

Based on the MD simulations, the polymyxin B loading mechanism of the erythrocyte liposomes is thus an electrostatic interaction between the positively charged polymyxin B and negative charges in the erythrocyte membrane. The insertion process then depends on membrane properties, as detailed in ref 10. The electrostatic attraction can be increased by adding additional negative charges in the form of the negatively charged lipid DMPS. Anchoring of the PmB in the erythrocyte membrane occurs when the fatty acid portion penetrates the membrane and aligns parallel to the membrane normal. The MD simulations provide a molecular mode of action: in the original erythrocyte membrane, the PmB molecules can attach

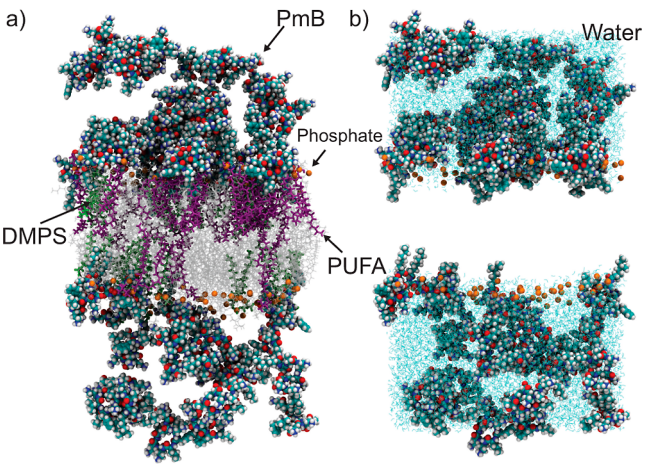

Figure 4. (a) Snapshot of MD simulations at 200 ns of hybrid erythrocyte membranes containing 5 mol % DMPS exposed to 20 mol % PmB. Highlighted are the phosphate groups (orange), PUFAs (purple), DMPS (green), and remaining membrane lipids (silver). (b) Side perspective with only water, phosphate groups, and PmB shown.

to the membrane, but they do not penetrate very deeply and the fatty acid tail of the PmB is tilted with respect to the membrane normal.

By adding 5 mol % DMPS to the erythrocyte membranes, most of the molecules appear to be anchored, with the PmB molecules deeply embedded in the head group region and the fatty acid tail reaching deep into the hydrophobic membrane core. Increasing the amount of negatively charged lipids should increase PmB retention further. However, it appears that the PmB can only penetrate the "soft" regions of the membrane, preferably in regions with polyunsaturated lipids. Increasing the anionic lipid fraction to 10 mol % does not increase the amount of anchored PmB molecules but contrarily results in attached PmB molecules as the membrane area containing polyunsaturated lipids is significantly reduced.

In terms of the loading capacity, increasing the number of PmB molecules does not necessarily increase the number of retained PmB molecules because the accessible area of the membrane is limited and so is the number of PmB molecules that can interact and anchor with the membrane. The MD results, therefore, support the experimentally determined optimal membrane composition and PmB loading.

To further support this hypothesis, the surface charge of the erythrocyte liposomes was confirmed experimentally by measuring the zeta potential. The zeta potential of pure erythrocyte liposomes (ghosts) was determined to be -25 ± 5 mV, of hybrid erythrocytes with 5 mol % DMPS to be -40 ± 5 mV, of hybrid erythrocytes with 5 mol % DMPS and 0.4 mol % PEG-MAL(2000) to be -6 ± 5 mV, and of erythro-PmBs (hybrid + DMPS + PEG + antibodies) to be -15 ± 5 mV. Following this data, erythrocyte liposomes have an initial surface charge. The negative charge increases with the incorporation of anionic DMPS, in agreement with the MD simulations. Charges appear to be shielded when PEG is incorporated, and the zeta potential drops and slightly increases again with antibody conjugation.

Antibodies can be Conjugated to Hybrid Erythrocyte Liposomes. The size distribution of liposomes at different stages of preparation [erythrocyte liposomes, RBC-DMPS hybrid erythrocyte liposomes, and RBC-DMPS-(PEG-MAL(2000))] (erythro-PmBs) was determined using dynamic

https://doi.org/10.1021/acsinfecdis.2c00017
ACS Infect. Dis. 2022, 8, 2059−2072

light scattering (DLS) and is shown in Figure 5. The erythrocyte liposomes showed an average size of 142 nm

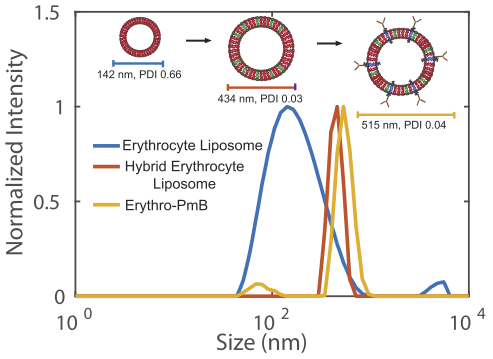

Figure 5. Liposome size determined through DLS at different stages of preparation of erythro-PmBs: erythrocyte liposome (blue), hybrid erythrocyte liposome (red), and erythro-PmB (yellow). Plotted is the normalized intensity as a function of particle size; data is reported as the mean size from $n = 3$. While erythrocyte liposomes showed an average size of 142 nm (PDI of 0.66), hybrid erythrocyte liposomes were 434 nm (PDI of 0.03) and erythro-PmBs were 515 nm in size (PDI: 0.04).

with a broad size distribution, as confirmed by a polydispersity index (PDI) of 0.66, corresponding to particle sizes ~40−900 nm. A significant increase in size to 434 nm was observed with the incorporation of the negatively charged DMPS, with a decreased PDI of 0.03. The incorporation of PEG-MAL(2000) and antibody conjugation to the maleimide groups (Erythro-PmB) increased the size to 515 nm (PDI 0.04). The large increase in size from erythrocyte liposomes to erythro-PmB suggests that antibodies were successfully conjugated to PEG-MAL(2000).

Erythrocyte liposomes show sizes between ~70 and 300 nm in atomic force microscopy (AFM) images in Figure 6a, consistent with the DLS results. The erythro-PmBs in Figure 6b have a size of ~800 nm, larger than the size determined with DLS (515 nm), likely due to a flattening of the liposomes on the silicon substrate. Although proteins cannot be observed at this resolution, the difference in surface characteristics, such as surface deformations along with inconsistencies in amplitude, may indicate the presence of antibodies on the membrane's surface.

The erythro-PmBs appear as burst liposomes with sizes of ~300 nm when imaged by transmission electron microscopy (TEM) in Figure 6c. The anti-*E. coli* antibodies were negatively stained using uranyl acetate such that the dark layer surrounding the erythro-PmBs can likely be attributed to the presence of proteins on the surface of the liposomes.

PmB Is Retained in Erythro-PmBs. The retention of PmB in the erythro-PmBs was quantified using dansyl-labeled PmB in a sedimentation assay. Figure 7a shows the UV images of 1 μL droplets (~1 mm diameter) of pure dansyl-PmB and pure hybrid erythrocyte liposomes (as controls), nonretained dansyl-PmB (the supernatant), and the erythro-PmBs (the pellet). The integrated fluorescence intensity is directly proportional to the amount of dansyl-PmB in the different samples, as plotted in Figure 7b. The intensity in the supernatant (the nonretained dansyl-PmB) was significantly reduced compared to the pellet (the amount of PmB retained in the erythro-PmBs). By comparing the different intensities, the loading efficiency was calculated to be 87 ± 3%, as detailed in the Materials and Methods. The retention of dansyl-PmB was further measured in a release assay over a period of 48 h at 37 °C, as shown in Figure 7c. The intensity of the total dansyl-PmB in the pellet (0 h) was found to be 2×10^6 counts/mm^2. No statistically significant change in fluorescent intensity was observed for the remaining time points, indicating that PmB continues to be retained in the membrane for at least 48 h.

Erythro-PmBs Show No Hemolytic Activity and No Nephrotoxicity *In Vitro*. The hemolytic activity of the erythro-PmBs is shown in Figure 8. Hemolysis was determined from hemoglobin release measured by UV absorption. Data are shown for free PmB and erythro-PmBs at different PmB concentrations from 0.25 MIC^f to 16 MIC^f. Values in the order of 0.06% were determined, well below the benchmark hemolysis rate of 2% identified by the American Society of Clinical Pathology,[30] and were considered to be nonhemolytic. Hemolytic activity of the erythro-PmBs at low concentration was less than that of free PmB, less than 0.01%, and independent of PmB concentration (within experimental error). Hemolytic activity was still small at the highest concentration, however, comparable to that of free PmB.

Nephrotoxicity was tested *in vitro* in renal membrane analogues. In this assay, a gold sensor mounted in a flow cell is first coated with renal membrane analogues and then treated with the agent, as pictured in Figure 9a. Detergent-susceptible (cholesterol-depleted) renal membranes were deposited on the sensors where membrane composition was taken from Marquéz *et al.*[31] The dielectric properties of the membrane layer were modeled by a series of resistors, a capacitor, and a Warburg element, sketched in Figure 9a.

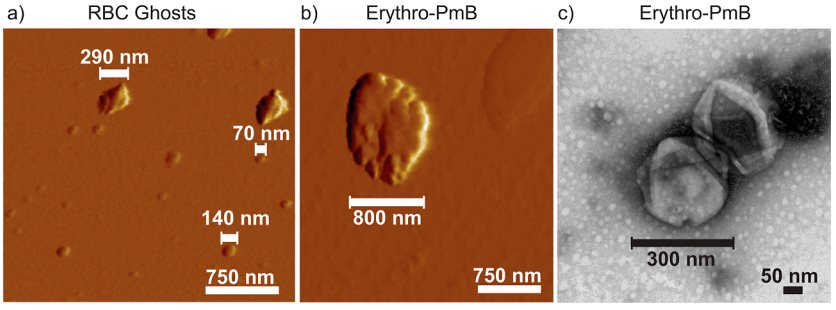

Figure 6. (a) Erythrocyte liposomes imaged by AFM. Liposomes between 70 and 300 nm were observed. (b) Erythro-PmBs imaged with AFM reveal a larger size with deformations in surface morphology. (c) Erythro-PmBs imaged by TEM appear as burst liposomes with sizes of ~300 nm with an external lipid and antibody layer. TEM images were obtained at 500,000× direct magnification.

https://doi.org/10.1021/acsinfecdis.2c00017
ACS Infect. Dis. 2022, 8, 2059−2072

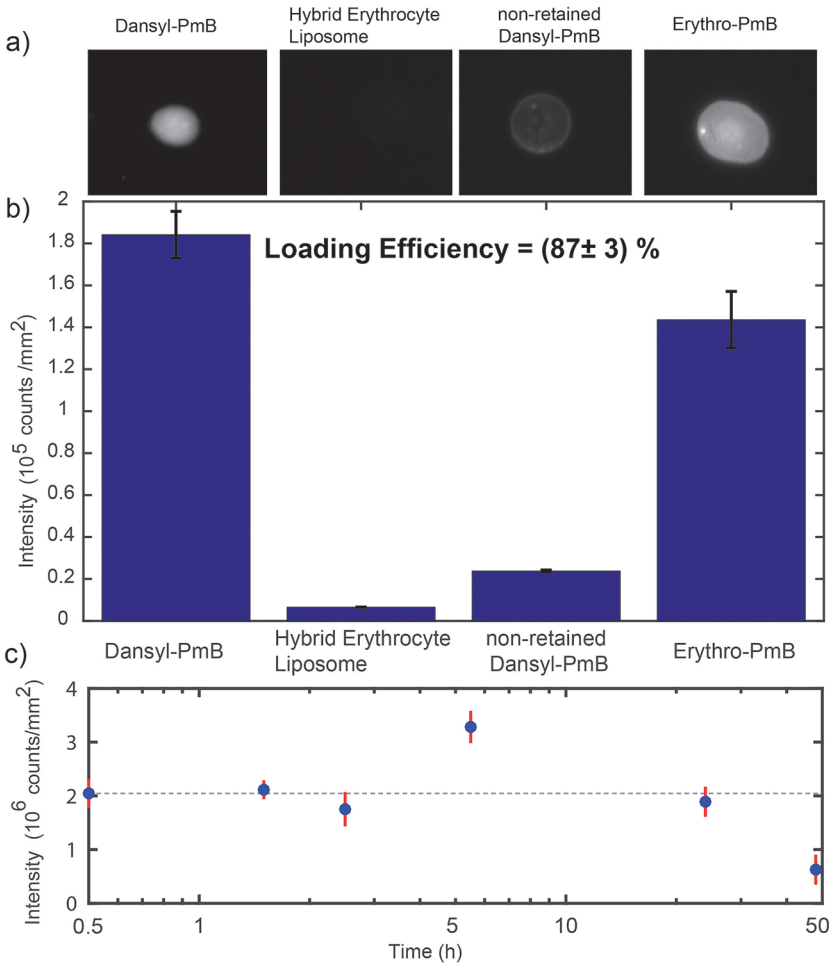

Figure 7. Retention of dansyl-PmB in erythro-PmBs. (a) Representative sample droplet images after 30 min of incubation of dansyl-PmB with erythro-PmBs under UV excitation at 365 nm. (b) Integrated pixel intensity for sample droplets. The loading efficiency was calculated as the ratio of PmB retained in the erythro-PmBs to the initial total dansyl-PmB in the solution. Data is averaged over $n = 3$. (c) Integrated pixel intensity for sample droplets under UV excitation at 365 nm for dansyl-PmB retained in the erythro-PmBs at different time points when incubated at 37 °C.

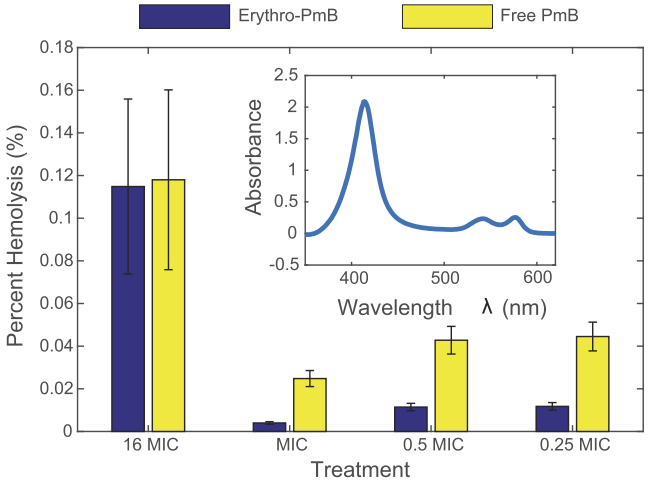

Figure 8. Hemolytic assay measuring the amount of hemolysis as a function of erythro-PmB concentration. Pure RBCs were treated with varying concentrations of (free) PmB as a positive control (MIC^f of 0.63 μg/mL). 12% Triton X-100 was used as a total lysis control, and PBS was used as a negative control.

Membranes were deposited as a passivating layer on the working Au electrode surface. The redox-active molecule ferricyanide was used as a reporter and added to the buffer used during the impedance experiments. When the membrane is intact, no current from the reduction or oxidation of the reporter is observed as the lipid membrane prevents the transfer of electrons at the electrode surface. When the membrane is damaged, the aqueous buffer (and therefore the reporter) can access the surface of the electrode. The membrane resistance was measured by electrochemical impedance spectroscopy (EIS). PmB, erythrocyte liposomes (the empty delivery system), and erythro-PmBs (antibody-conjugated erythrocyte liposomes with polymyxin B) were then run through the flow cell, and membrane resistance (R_m) was recorded as a function of time.

R_m initially increased when lipid solution was run through the flow cell and a membrane formed on the sensor. We used susceptible renal membrane analogues containing 3 mol % cholesterol as they are most sensitive to PmB damage.[13] The solution is then switched, and a buffer containing polymyxin B at a concentration of 25 μg/mL is pumped through the cell. As shown in Figure 9b, the resistance continues to increase, indicating that PmB attaches to the surface of the membranes. Once a critical PmB concentration is achieved, the R_m drops down as a result of break through and pore formation in the membranes.

https://doi.org/10.1021/acsinfecdis.2c00017
ACS Infect. Dis. 2022, 8, 2059−2072

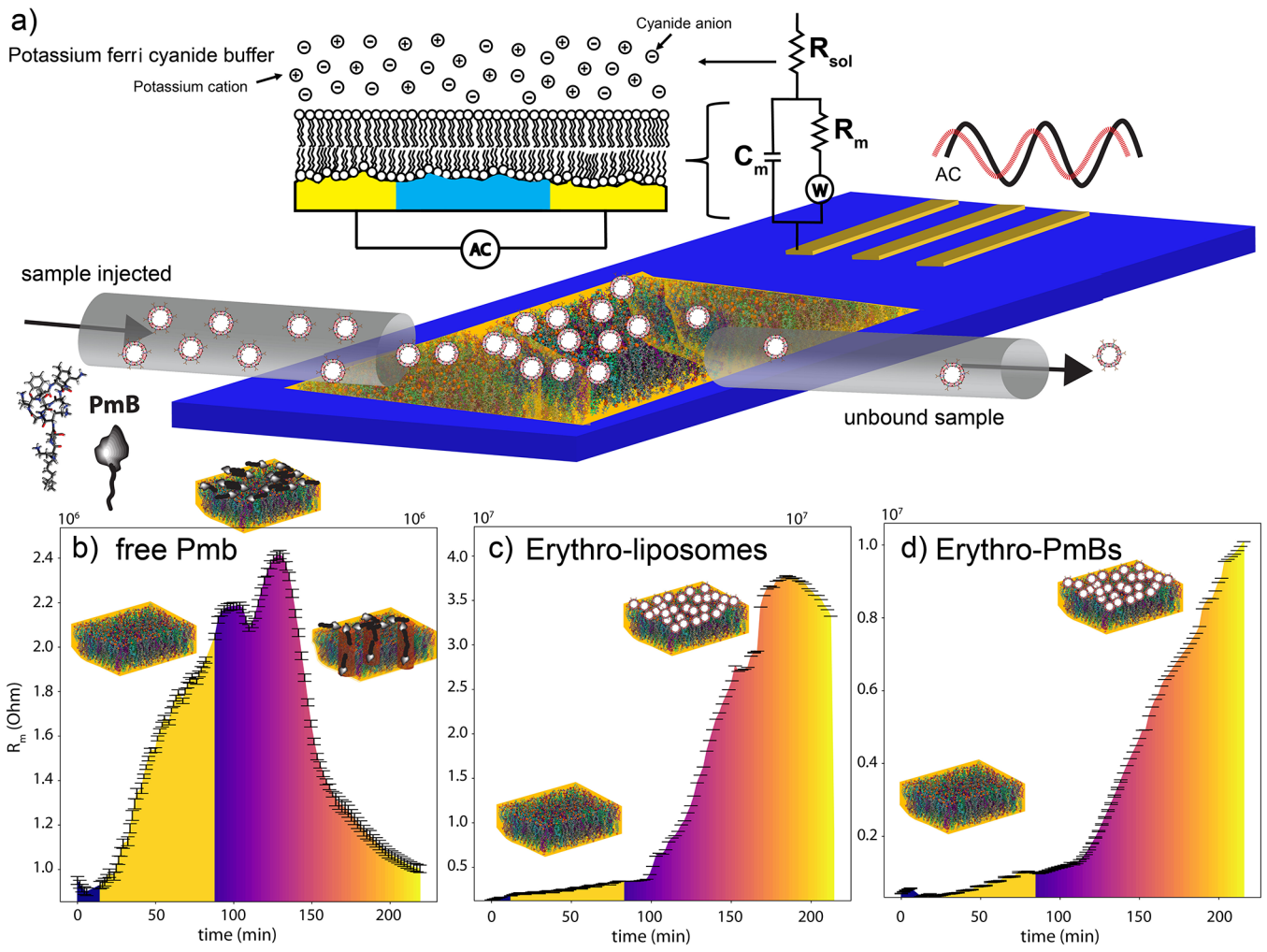

Figure 9. (a) Renal membrane analogues were formed on a gold sensor, and dielectric membrane properties were measured by EIS. Membrane resistance (R_m) is a very sensitive measure to detect membrane damage as this resistance drops when pores form and the redox-active molecule ferricyanide can reach the electrode. (b) For free PmB, R_m initially increases when the membrane is formed on the sensor. When treated with PmB, the PmB molecules start to accumulate on the membrane surface and resistance increases before sharply dropping as a result of membrane damage. (c) When exposed to erythrocyte liposomes, the increase of R_m is indicative of liposomes attaching to the membrane on the sensor. (d) For erythro-PmBs, R_m keeps increasing as a result of liposome attachment. There is no drop in resistance, which would be indicative of membrane damage.

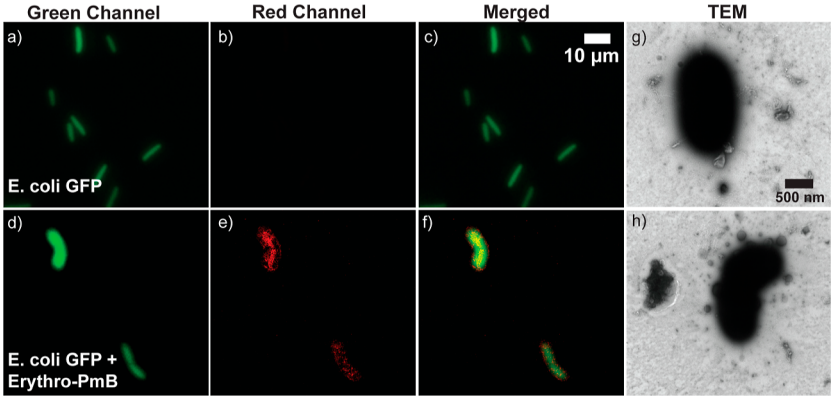

Figure 10. Erythro-PmBs target and interact with *E. coli*. (a–c) show *E. coli*-GFP imaged with fluorescence microscopy. The emission appears in the green channel only. (d–f) show *E. coli*-GFP incubated with erythro-PmBs whose membranes were labeled with Texas Red (TR-DHPE). Green and red channels in (d,e) show bacteria and erythro-PmBs, respectively. Erythro-PmBs (red) surround and attach to the bacteria (green) in the merged channel in (f). (g,h) Erythro-PmBs were incubated with *E. coli* bacteria, stained with uranyl acetate, and imaged by TEM at 25,000× direct magnification. The erythro-PmBs were found surrounding and attaching to the *E. coli*.

https://doi.org/10.1021/acsinfecdis.2c00017
ACS Infect. Dis. 2022, 8, 2059–2072

When using erythrocyte liposomes (in Figure 9c), R_m increases after membrane formation indicative of liposome attachment to the renal membrane analogue. Resistance stays high, indicating that the membrane stays intact. When treating the sensor with erythro-PmBs, resistance continuously increases after membrane formation with no sign of leakage and membrane damage. Hence, while free PmB showed clear nephrotoxicity and damage to renal membrane analogues, the erythrocyte liposomes and the erythro-PmBs did not result in damage in the susceptible (cholesterol-depleted) renal membranes.

Erythro-PmBs Target *E. coli* Bacteria. *E. coli* expressing green fluorescent protein (GFP) were fixed onto agarose pads and imaged with epifluorescence microscopy as shown in Figure 10a–c. The bacteria appear rod-like and exhibit an average diameter of ∼2 μm and length of ∼10 μm with strong fluorescence emitted in the green channel, only. *E. coli*-GFPs were then incubated with erythro-PmBs whose membranes were labeled with Texas Red (TR-DHPE), as shown in Figure 10d–f. Bacteria and erythro-PmBs are observed with the green and red channels, respectively. In the merged channel (f), erythro-PmBs (red) surround and interact with the *E. coli*-GFP. The yellow color is indicative of erythro-PmB colocalization.

E. coli were incubated with erythro-PmBs for 1 h at 37 °C, stained with uranyl acetate to increase contrast, and imaged by TEM, as shown in Figure 10g,h. The erythro-PmBs were found to concentrate around the *E. coli* and form attachments to the bacterial surface. Several erythro-PmBs appear to have made contact with the bacteria.

Erythro-PmBs Effectively Deliver PmBs to *E. coli* Bacteria. Bacterial growth curves for *E. coli* for different concentrations of (free) PmB (MIC^f, 0.5 MIC^f, 0.25 MIC^f, and 0 MIC^f) are shown in Figure 11a. Based on these experiments, the MIC^f was determined to be 0.63 μg/mL. Absorbance at 600 nm (OD 600) was measured during a period of 24 h. In the absence of antibiotics (0 MIC), bacteria grow monotonically and demonstrate a characteristic diauxic growth curve with two exponential growth cycles: (1) the bacteria begin to grow with glucose metabolism and switch to (2) lactose utilization after about 14 h.[32] Bacteria treated with 0.25 MIC^f behaved similarly. A lag phase was observed before the first exponential cycle after the addition of an intermediate concentration of 0.5 MIC^f, where exponential growth was delayed by ∼9 h. No growth was observed at the MIC^f of PmB.

Growth curves for *E. coli* treated with varying concentrations of erythro-PmBs containing MIC^f, 0.5 MIC^f, 0.25 MIC^f, and 0 MIC^f of PmB are shown in Figure 11b. While *E. coli* showed similar initial exponential growth for erythro-PmBs compared to free PmB at 0 MIC^f and 0.25 MIC^f, the initial lag phase was increased by about ∼5 h at 0.5 MIC^f of erythro-PmBs. No growth was observed at MIC^f.

Erythro-PmBs Are Selective. Bacterial growth curves for *K. aerogenes* for different concentrations of (free) PmB (MIC^f, 0.5 MIC^f, 0.25 MIC^f, and 0 MIC^f) are shown in Figure 12a.

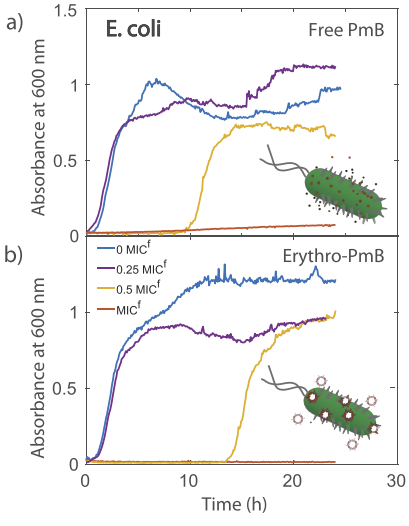

Figure 11. Bacterial growth curves measured at 600 nm (OD600) over 24 h for *E. coli* at various treatment concentrations. (a) *E. coli* were treated with free PmB and the minimum concentration was determined to be 0.63 μg/mL (MIC^f). (b) Various orders of the MIC^f were delivered in the erythro-PmBs. Growth curves for erythro-PmBs show an overall similar behavior as for free PmB, indicating that the erythro-PmBs are as efficient as free PmB in inhibiting *E. coli* growth.

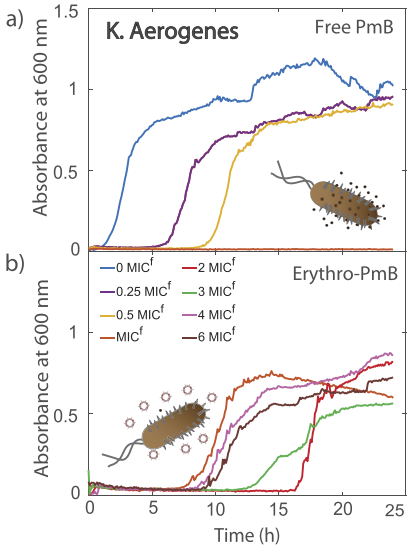

Figure 12. Bacterial growth curves measured at 600 nm (OD600) over 24 h for *K. aerogenes* with various treatment concentrations. (a) *K. aerogenes* were treated with free PmB, and the minimum inhibitory concentration (MIC^f) was determined to be 1.5 μg/mL. The lengths of the lag phase decreased monotonously with decreasing PmB concentration, similar to *E. coli*. (b) Different orders of the MIC^f were delivered in the erythro-PmBs. The MIC for the erythro-PmBs (MIC^E) was significantly increased to more than 6 MIC^f, indicating that erythro-PmBs do not deliver PmB efficiently to *K. aerogenes*.

The MIC^f for *K. aerogenes* was determined to be 1.5 μg/mL. Similar to *E. coli*, *K. aerogenes* exhibit a diauxic growth curve at 0 MIC^f, with a second exponential growth phase occurring at ∼14 h. Diauxic growth was less evident in the presence of free PmB: 0.25 MIC^f to MIC^f. *K. aerogenes* treated with intermediate concentrations of the MIC^f showed a prolonged lag phase: 0.25 MIC^f (6 h) and 0.5 MIC^f (9 h).

Bacterial growth curves for *K. aerogenes* treated with erythro-PmBs containing anti-*E. coli* antibodies are shown in Figure 12b. While no growth was observed at the MIC^f for free PmB, *K. aerogenes* showed a delay in growth by ∼7 h in the presence of erythro-PmBs. Delayed growth (with lag times of up to ∼16 h) continued to be observed at concentrations of 2 MIC^f, 3 MIC^f, 4 MIC^f, and up to 6 MIC^f, such that the MIC^E was

https://doi.org/10.1021/acsinfecdis.2c00017
ACS Infect. Dis. 2022, 8, 2059–2072

defined as >9 μg/mL. The MIC values for *E. coli* and *K. aerogenes* treated with free PmB and erythro-PmBs are listed in Table 1. While no change in MIC was observed for *E. coli*, the MIC increased by more than 6-fold for *K. aerogenes* treated with erythro-PmBs.

Table 1. MIC Was Recorded as the Minimum Concentration Required to Inhibit Bacterial Growth Over a 24 h Period[a]

	MIC (μg/mL)	
	free PmB	Erythro-PmB
E. coli	0.63	0.63
K. aerogenes	1.5	>9

[a]Bacterial growth was analyzed by measuring bacterial growth curves at 600 nm (OD600) of bacteria treated with either free PmB or erythro-PmBs. While MIC for *E. coli* was the same for free PmB and erythro-PmBs, MIC for K. aerogenes was significantly increased to >6 MIC.

DISCUSSION

Typical loading efficiencies of liposomal PmB have been reported to be on the order of a few percent[33,34] for synthetic liposomes made of dipalmitoylphosphatidylcholine/cholesterol and palmitoyloleoylphosphatidylcholine/cholesterol. Higher entrapment efficiencies of ∼50% were achieved with mixtures of varying phosphatidylcholine, sphingomyelin lipids, and cholesterol.[35] We report substantially higher loading efficiencies of erythro-PmBs of ∼90%. In contrast to the results obtained with synthetic liposomes,[35] the inclusion of 5 mol % DMPS increased the loading efficiency of the erythro-PmBs, which points to electrostatic interactions between the negatively charged membrane and the cationic PmB. Such a relation between membrane charge and PmB efficacy has been reported in bacterial membrane mimics.[10] While higher membrane charge should further increase PmB retention, increasing the DMPS fraction in the erythrocyte liposomes from 5 to 10% reduced retention.

MD simulations provide a detailed picture of the PmB loading and retention mechanism: the cationic PmB molecules are attracted to the erythrocyte membranes through negatively charged lipid molecules. Anchoring of the PmB molecules in the membranes occurs through the insertion of their acyl tail into the hydrophobic membrane core. This insertion preferably happens in softer membrane areas with higher densities of PUFAs. While increasing the anionic DMPS fraction increases the number of PmBs attracted to the membranes, they are unable to fully insert because at the same time the softer, PUFA-rich membrane areas decrease. Based on this mechanism, the optimal amount of negative charges was found to be 5 mol % DMPS. While PmB leads to significant damage in bacterial membranes upon insertion, the presence of cholesterol in eukaryotic plasma membranes was reported to prevent membrane collapse[13] as the stiff cholesterol molecules serve to stabilize the bilayer structure. The membranes of the erythro-PmBs can thus carry PmB without liposome perforation or rupture.

The MIC of synthetic liposomal PmB was reported to depend on the amount of free drug in solution, and the effect of the liposomes was mainly to increase PmB diffusion.[35] In that model, a higher ratio of liposome to PmB would enhance liposome−bacteria interaction. Increasing the relative amount of PmB did not increase the retention of PmB in the erythro-PmBs. Based on the MD simulations, when exposing the erythrocyte liposomes to larger concentrations of PmB, the soft, PUFA-rich areas of the membrane are saturated with PmB molecules and most of the molecules can no longer directly interact with the erythrocyte membranes. We suggest that the optimal loading capacity of PmB is around 1000 PmB molecules per liposome. In this case, the high MIC^E values for *K. aerogenes* indicate that the amount of freely diffusing PmB is small and that PmB is effectively retained with erythro-PmBs, even over long periods of time (>48 h).

Erythro-PmBs were found to efficiently deliver PmB to *E. coli* (ATCC: 10798) with the same efficacy (identical MIC^f value of 0.63 μg/mL) as free PmB. We did not find evidence that the conjugation of antibodies enhances PmB delivery to *E. coli*. This is contradictory to a previous study where *in vitro* and *in vivo* liposomal PmB delivery was tested against resistant Gram-negative bacterial strains and was found to reduce the MIC by a factor of 4.[33,34] We note that resistant bacterial strains often show alterations in membrane lipid composition leading to changes in membrane charge and density, which severely limits their susceptibility to free PmB.[5] Elevated concentrations of PmB are then required; the MIC for *E. coli* (ATCC 25922), for instance, was reported to be 8.0 μg/mL.[33] On the other hand, liposomal PmB delivery only required 2 μg/mL, making liposomes advantageous in this case.

Antibodies have been previously conjugated to nanoparticles. For instance, polymeric nanoparticles with antibodies against *Staphylococcus aureus* conjugated on the surface were found to preferentially bind to *S. aureus* as opposed to *Pseudomonas aeruginosa* and exhibited higher target binding than nanoparticles lacking the antibody.[36] This led to a significant improvement in treatment efficacy when delivering rifampin *in vivo*. Similarly, in our case, antibody conjugation significantly enhanced the specificity of erythro-PmBs as PmB was not effectively delivered to bacteria lacking the corresponding antigens. Both *E. coli* and *K. aerogenes* were susceptible to PmB, with MIC^f values of <2 μg/mL.[37] While *E. coli* showed no change in susceptibility when treated with erythro-PmBs, the MIC for *K. aerogenes* increased to >9 μg/mL, significantly greater than the resistant breakpoint of 4 μg/mL.[37] This makes the erythro-PmBs a selective platform for the delivery of PmB to bacterial targets. The high retention and correspondingly small amounts of free PmB at the same time minimize potential toxicity.

Delivery of PmB to bacteria can be achieved through different mechanisms: fusion of liposomes with the target membrane, adsorption of liposomes, lipid exchange, or endocytosis.[38] Fluid liposomes composed of dipalmitoylphosphatidylcholine/dimyristoylglycerophosphoglycerol have been shown to fuse with *P. aeruginosa*, allowing the intracellular release of encapsulated tobramycin.[39] If our erythro-PmBs acted through diffusion, the presence of erythro-PmB in close proximity to a *K. aerogenes* bacterium would likely promote drug delivery. However, this is not evident in our data, as even at high erythro-PmB concentrations, where there is a high probability for an interaction to occur, the bacteria were still able to grow. Our findings, therefore, rather suggest fusion or lipid exchange for PmB to be delivered. Given that PmB is strongly associated with erythro-PmBs, this promotes localized PmB release at the targeted site of infection. This hypothesis is also supported by the electrochemical impedance data in the nephrotoxicity assay. Both, the pure erythrocyte liposomes,

https://doi.org/10.1021/acsinfecdis.2c00017
ACS Infect. Dis. 2022, 8, 2059−2072

and the erythro-PmBs were found to attach to the renal analogue membranes, without leading to membrane damage. However, the erythro-PmBs did not release PmB, which would be detected as damage to the cholesterol-depleted renal membranes. Liposomes lacking the antibody may still fuse with the bacterial membrane; however, this fusion would happen spontaneously in the chance that the liposome and bacterial membrane come into close contact. This may explain the presence of the lag phase in *K. aerogenes* treated with high doses of the erythro-PmBs made specific to *E. coli*. While the growth was slightly delayed, doses higher than the MIC were unsuccessful in completely inhibiting growth. Hence, while we cannot unambiguously determine the PmB delivery mechanism at this point, the experimental findings seem to rule out a simple diffusion of PmB molecules in favor of a fusion or lipid exchange mechanism. However, further studies, likely using labeled lipid molecules and labeled PmB, are required to clarify this point.

While all liposome samples used in this study have been freshly prepared (<3 days), erythrocyte liposomes and the erythro-PmBs were found to be stable when refrigerated for at least 2 weeks. Studies have shown that negatively charged lipids can aid in preventing liposome aggregation in solution and circulation;[40] however, they have a higher chance of being taken up by the host's immune system in comparison to neutral and positively charged liposomes.[41] Moreover, the incorporation of PEG shields the liposome by creating a hydration layer, resulting in reduced clearance of the liposomes. The erythro-PmBs have not been tested in animals at this point such that we cannot comment on their fate in an organism. However, we note that erythrocyte-based virus-like particles have been prepared using a similar protocol in our lab[42] and tested in mouse models. These erythro-VLPs were injected intravenously and stable in the mice for at least 2 weeks. We speculate that also the erythro-PmBs will show similar biocompatibility and stability in animal studies.

There is potential for the RBC-based PmB delivery system presented in this paper to be transferable to other antimicrobials; however, some considerations need to be addressed. First, one would need to investigate the interaction of the antimicrobial with the erythrocyte membrane to determine whether modifications in the encapsulation protocol are necessary. PmB interacts directly with the membrane and could be retained on the liposomal surface; however, other antimicrobials, such as hydrophilic drugs, may need to be encapsulated within the liposome's aqueous core. Second, the properties of the antimicrobial need to be taken into consideration, such as the antimicrobial stereochemistry, molecular size, and charge, to optimize the hybrid erythrocyte membrane with the incorporation of synthetic lipids that will allow for high loading efficiency without compromising membrane stability.

CONCLUSIONS

We show that antibody-conjugated hybrid erythrocyte liposomes are an effective platform to selectively deliver PmB to bacterial targets. Hybrid erythrocyte liposomes were formed through the inclusion of negatively charged DMPS to maximize the retention of the cationic PmB. Anti-*E. coli* antibodies were conjugated by the inclusion of DSPE-PEG maleimide linkers. These erythro-PmBs deliver PmB to *E. coli* as efficiently as free PmB, with identical MIC values. They are, however, selective as the MIC for *K. aerogenes* increased 6-fold, well beyond the resistant breakpoint. Combined with the high loading efficiency of ∼90%, these erythro-PmBs represent a selective platform for the delivery of PmBs to bacterial targets.

MATERIALS AND METHODS

This research was approved by the Hamilton Integrated Research Ethics Board (HIREB) under approval number 1354-T. Informed consent was obtained from all blood donors. The authors confirm that all methods were performed in accordance with the relevant guidelines and regulations.

Preparation of Erythrocyte Liposomes. The detailed protocol is described elsewhere.[43] In brief, heparinized blood samples were collected. The blood was washed twice, and the RBCs were isolated by successive centrifugation and replacement of the supernatant with phosphate-buffered saline (PBS). The cells were exposed to osmotic stress by mixing the hematocrit with the lysis buffer (3% PBS, pH 8) at a concentration of 5 vol %. The lysis buffer was prechilled to ∼4 °C, and the reaction tubes were immediately stored on ice to prevent a fast reclosing of the ruptured cells. Hemoglobin and other cellular components were removed through multiple washing steps as described in ref 43. The protocol results in a white pellet containing closed empty erythrocyte liposomes.

The resulting solution was tip sonicated 20 times for 5 and 55 s breaks each at a power of 100 W. The reaction tube was placed on ice during sonication to prevent the sample from overheating. Afterward, the tube was centrifuged for 15 min at 20,000*g*. The supernatant consisted of a solution of small, nanometer-sized liposomes and is hereafter referred to as the *Erythrocyte Liposome Solution*. The protocol results in a membrane concentration of ∼14 mg/mL.[43]

Preparation of Erythro-PmBs. Individual stock solutions of synthetic lipids were prepared by dissolving 1,2-distearoyl-*sn*-glycero-3-phosphoethanolamine-*N*-[maleimide-(polyethylene glycol)-2000] (PEG-MAL(2000), Avanti) in chloroform and 1,2-dimyristoyl-*sn*-glycero-3-phospho-L-serine (DMPS, Avanti) in chloroform and 2,2,2-trifluoroethanol (TFE) (1:1). To produce a hybrid RBC membrane, the lipids were added to a separate glass vial to achieve an overall lipid composition of 0.4 mol % PEG-MAL(2000) and 5 mol % DMPS. The chloroform was removed by light nitrogen flow in the glass vial for ∼20 min before resuspending the synthetic lipids in the *Erythrocyte Liposome Solution*. The mixture was then vortexed and incubated for 30 min to ensure that all of the synthetic lipids had been removed from the bottom surface of the glass vial. The hybrid membrane mixture was then sonicated at 20% intensity with 5 s pulses and 55 s breaks for 20 min in an ice bucket. The sample was dried completely using a Vacufuge and incubated at 37 °C for 1 h at 97% relative humidity (RH). This step allows the lipids to anneal and form a homogeneous membrane as previously shown.[44] Following incubation, dilute PBS was added to achieve an overall molar concentration of ∼30 nM. This will be referred to as the *hybrid membrane solution*.

Rabbit anti-*E. coli* antibody with an IgG concentration of 4.0 mg/mL in 0.1% sodium azide was purchased from Bio-Rad (Product Code: 4329-4906). The *antibody solution* was aliquoted into four tubes each containing 1 mg of antibody and stored at −20 °C. Since sodium azide is toxic to bacteria, a buffer exchange was done with PBS prior to RBC conjugation. The 250 μL *antibody solution* was centrifuged at 12,000*g* for 15 min in a 0.5 mL Amicon Ultra Centrifugal Filter Unit (Product Code: UFC501008) with a molecular weight cutoff of 10 kDa.

https://doi.org/10.1021/acsinfecdis.2c00017
ACS Infect. Dis. 2022, 8, 2059−2072

The filtrate was removed, and the residue was resuspended to the original volume of PBS. This step was repeated three times to ensure the complete removal of all sodium azide. Once all washing was complete, the filter tube was turned upside down into a clean collecting tube, centrifuged for 5 min at 12,000*g*, and resuspended to the original volume of PBS. The concentration before and after washing was measured on a nano-spectrophotometer at 260 nm, which confirmed >90% protein recovery.

The *antibody solution* was then incubated for 20 min in 100× excess of TCEP at room temperature. This step reduces the antibody's disulfide bonds, preparing them for conjugation to PEG-MAL(2000). The *antibody solution* was then added to the *hybrid membrane solution* and incubated at room temperature for 1 h and overnight at 4 °C. Following incubation, the unbound antibody was removed through centrifugation at 12,000*g* for 2 h.

PmB was then introduced into the resulting solution at a ratio of 1000:1. The mixture was allowed to incubate for 30 min at 4 °C before centrifuging for 4 h at 20,000 ×*g*. The supernatant containing free PmB was removed and replaced with PBS to produce the final erythro-PmBs.

DLS and Zeta Potential. A Zetasizer Nano ZS from Malvern Panalytical was used to determine the size distribution of the liposomes. The instrument is equipped with a 4 mW He−Ne laser (wavelength: 633 nm) and noninvasive back-scattering optics. The diffusion constant, D, of the liposomes was determined by measuring the DLS spectrum. This is related to the particle size *via* the Stokes−Einstein relation: $D = \frac{k_B T}{6\pi\eta r}$, where η is the dynamic viscosity of water, k_B is the Boltzmann constant, T is the sample temperature, and r is the radius of a spherical particle. All measurements were performed at 25 °C on 1 mL of the sample containing ≈0.5 mg/mL of membrane material in DTS0012 cuvettes.

The polydispersity index (PDI) was calculated as

$$\mathrm{PDI} = \left(\frac{\sigma}{d}\right)^2 \tag{1}$$

where σ is the standard deviation and d is the peak center of the size distribution.

The zeta potential was determined by laser doppler micro-electrophoresis. Here, an alternating electric field is applied to the solution, and the velocity of the particles is determined *via* the patented phase analysis light scattering (M3-PALS, patent reference: US7217350). This allows for the determination of the charge-dependent mobility of the particles. All measurements were performed at 25 °C on 1 mL sample containing ≈0.5 mg/mL of liposomes.

Preparation of Bacterial Overnight Cultures. *E. coli* (ATCC 10798) and *K. aerogenes* (ATCC 35029) were grown in Luria−Bertani (Miller) growth media containing NaCl (10 g/L), tryptone (10 g/L), and yeast extract (5 g/L) purchased from Millipore Sigma. Overnight cultures containing bacterial culture and LB broth (10:1000) were incubated at 37 °C for 24 h in a shaking incubator.

Ampicillin-resistant GFP-*E. coli* (ATCC 25922GFP) were grown in tryptic soy media (pH 7.3) containing casein peptone (17 g/L), soya peptone (3 g/L), NaCl (5 g/L), dipotassium hydrogen phosphate (2.5 g/L), glucose (2.5 g/L), and ampicillin (100 μg/mL). Overnight cultures were prepared following the same procedure as above.

Minimum Inhibitory Concentration. Bacterial growth for *E. coli* and *K. aerogenes* was analyzed by measuring optical density at 600 nm every 5 min over a 24 h period using a nano-spectrophotometer set to 37 °C. Reaction mixtures containing 10 μL of bacterial overnight culture, the required treatment, LB to a total volume of 1 mL were prepared. To find the MIC, bacteria were treated with varying concentrations of free PmB to determine which concentration is the most effective at preventing bacterial growth. This concentration is referred to as the MIC: *E. coli* (0.63 μg/mL) and *K. aerogenes* (1.5 μg/mL).

The same method was used to test the activity of the erythro-PmBs. The volume of required erythro-PmB treatment was determined such that the number of administered PmB molecules was equivalent to the concentrations used in the free PmB treatment: MIC, 0.5 MIC, and 0.25 MIC.

Epifluorescence Microscopy. Fluorescently labeled membranes were prepared by doping the bilayers with Texas Red 1,2-dihexadecanoyl-*sn*-Glycero-3-Phosphoethanolamine (TR-DHPE, Thermo Fisher, Catalog number: T1395MP) which was used previously as an indicator for liquid disordered l_d domains.[45−48] TR-DHPE was mixed with the synthetic lipids PEG-MAL(2000) (0.4 mol %) and DMPS (5 mol %) to achieve an overall lipid composition of 0.015 mass %. The synthetic lipids were mixed with the RBC membranes following the same protocol described earlier.

A 1% agarose solution was used to prepare agarose pads. The agarose was allowed to solidify in a chamber composed of glass slides and was sandwiched by placing another glass slide on top of the mixture. After 45 min, the agarose was cut into 2 × 2 cm^2 pads. Overnight cultures of GFP-*E. coli* grown to ∼1 OD were incubated with stained erythro-PmBs at a ratio of 1:9 for 3 h at room temperature before fixation onto the agarose pads. A cover glass was mounted on top.

Epifluorescence microscopy was conducted using a Nikon Eclipse LV100 ND microscope. The instrument was equipped with a Plan Fluor BD 40× objective with a numerical aperture of 0.75. Images were recorded using a Nikon DS-Ri2 camera with a resolution of 4908 × 3264 pixels and a pixel size of 7.3 × 7.3 μm. The camera was mounted *via* a 2.5× telescope to the microscope. All images were recorded in episcopic illumination mode using a halogen lamp. Images were recorded using Nikon control software (NIS Elements, Version 4.60.0).

Atomic Force Microscopy. Samples were prepared on silicon wafers prior to imaging with AFM. The silicon wafers were first treated with dichloromethane for 20 min to remove organic contamination and then rinsed with water and methanol. The silicon wafers were then further cleaned with a plasma cleaner in 1 mbar at 80:20 nitrogen/oxygen for 1 min. This step leaves the surface of the silicon wafer in a hydrophilic state, allowing the adhesion of the liposomes. The silicon wafers were dipped into a diluted liposome mixture (1:1000, 0.03 nM) for 15 s and rinsed with ultrapure water to remove any unbound material. The sample was left to air dry before imaging.

AFM was conducted using a Nanomagnetics ezAFM+ microscope. The instrument uses a field-programmable gate array-based digital feedback control and is able to scan an area of 40 × 40 μm^2 with a maximal height difference of 4 μm. Samples were prepared on silicon wafers and taped on a steel plate, which was then magnetically mounted on a 38 mm motorized XY-stage. A digital microscope with a field of view of 390 × 230 μm^2 was focused either on the cantilever or

https://doi.org/10.1021/acsinfecdis.2c00017
ACS Infect. Dis. 2022, 8, 2059−2072

sample surface and allowed aligning the specimen with respect to the cantilever tip. All scans were completed in noncontact (tapping mode). The instrument was equipped with an AppNano N-type Long-Cantilever Al Reflex Coating probe. The tip had a radius of less than 10 nm, a spring constant of 36−90 N/mm, and a frequency range of 160−225 kHz.

The PDI parameters were kept constant at 11, 1, and 10%, with a set point of 50%, and an oscillation amplitude of ∼2.2 V (∼190 kHz). An area on the sample surface was first chosen using a digital microscope and the motorized stage. Afterward, a coarse scan was performed over an area of 20 × 20 μm^2 with a scanning speed of 10 μm/s at a resolution of 512 × 512 px. A higher-resolution scan was then completed on a single liposome with a scanning speed of 1 μm/s at a resolution of 1024 × 1024 px. Image analysis was done on NanoMagnetics Image Analyzer Software (version 1.4). Mean and median filters were applied to enhance liposome contrast.

Electron Microscopy. Erythro-PmBs were prepared and diluted to ∼0.2 mg/mL in diluted PBS. The erythro-PmBs were then fixed onto formvar grids and negatively stained with 1% uranyl acetate for 30 s. Electron microscopy was done using a JEOL TEMSCAN electron microscope at the Canadian Centre for Electron Microscopy. Images were taken at 500,000× direct magnification.

Overnight *E. coli* bacterial cultures were grown to an OD of ∼0.9 and were mixed with erythro-PmBs at a ratio of 1:1000 with an overall erythro-PmB concentration of ∼0.2 mg/mL. The samples were imaged at 25,000× direct magnification following the same procedure for the individual erythro-PmBs.

Retention Assay. To determine the percentage of PmB molecules that were retained in the erythro-PmBs, a dansyl-labeled PmB was mixed with the hybrid erythrocyte liposomes at 8000× excess following the previously mentioned protocol. The mixture was allowed to incubate for 30 min at 4 °C before centrifuging for 4 h at 20,000*g*. The pellet contains the erythro-PmBs that contain the retained dansyl-PmB. The supernatant, containing the nonretained dansyl-PmB, was removed. A dansyl-PmB control was used with the same concentration of dansyl-PmB without erythro-PmBs. Small droplets (1 μL) of the supernatant, pellet, pure hybrid erythrocyte liposomes, and dansyl-PmB were imaged using an Azure Biosystems c400 Imaging system at an UV excitation of 365 nm.

A release assay at 37 °C was done by preparing the erythro-PmBs with dansyl-PmB. To separate the free dansyl-PmB, the mixture was centrifuged through at 12,000*g* for 15 min using a 0.5 mL Amicon Ultra Centrifugal Filter Unit (Product Code: UFC501008) with a molecular weight cutoff of 10 kDa. The free dansyl-PmB found in the filtrate was collected and the residue, containing the erythro-PmBs, was resuspended to the original volume in dilute PBS. Small droplets (1 μL) of the erythro-PmBs and free dansyl-PmB were imaged at the following time points: 30 min, 1.5 h, 2.5 h, 5.5 h, 24 h, and 48 h.

Image analysis for both the retention and release assay was completed using ImageJ. An image mask was created by enhancing the contrast of the droplet (2.5 saturated pixels, normalized). The image was smoothed using the built-in smooth function, and autothresholding was completed using the Yen thresholding method to produce the final mask. The mask was then combined with the original droplet image and converted to 16-color. The pixel intensity was measured for each droplet area.

The retention (%) was calculated by

$$\text{retention}(\%) = \left| \frac{I_{\text{control}} - I_{\text{supernatant}}}{I_{\text{control}}} \right| \times 100 \quad (2)$$

Regarding the data in Figure 7, when compared to the pure dansyl-PmB reference, the pellet comprised 78% of the total fluorescence signal, while the nonretained dansyl-PmB contributed 13% (fluorescent intensity of pure hybrid erythrocyte liposomes 4%). The retention was thus calculated from these values to be (87 ± 3)%.

Hemolysis Assay. Hemolysis of the erythro-PmBs was measured in reaction tubes containing 1 mL of the hematocrit solution at the concentrations of 16 MIC (10 μg/mL), MIC, 0.5 MIC, and 0.25 MIC in a total reaction volume of 1.2 mL. PmB, 12% Triton X-100, and PBS were used as a positive and negative control. The samples were incubated for 1 h at 37 °C on an orbital shaker before being centrifuged at 20,000*g* for 1 h. The absorption spectra of the supernatant, containing the released hemoglobin, were measured from 200 to 900 nm using UV−visible light spectroscopy with a nanophotometer from IMGEN.

The absorption spectra were integrated from 350 to 620 nm to capture the characteristic hemoglobin absorption peaks at 416.4, 514, and 577 nm. The percentage of hemolysis was calculated as

$$\text{percent hemolysis}\ (\%) = \left| \frac{A_{\text{RBC}} - A_{\text{PBS}}}{A_{\text{Triton}} - A_{\text{PBS}}} \right| \times 100 \quad (3)$$

where A is the integrated area.

Electrochemical Impedance Spectroscopy. Potential nephrotoxicity was tested *in vitro* by measuring EIS in renal membrane analogues. Lipid compositions were based on the composition of detergent-susceptible (cholesterol-depleted) renal membranes by Marquéz *et al.*[31] 1,2-Dimyristoyl-*sn*-glycero-3-phosphocholine (DMPC), -phospho-L-serine (DMPS), and -phosphoethanolamine (DMPE) (Avanti Polar Lipids) (2:1:1 mol %), cholesterol (Caledon), and polymyxin B (Sigma-Aldrich) were mixed at desired molecular ratios and dissolved in a mixture of chloroform (Caledon)/2,2,2-trifluoroethanol (TFE) (Sigma-Aldrich). 3 mol % cholesterol was added to the lipid mix, resulting in a 2:1:1:0.2 ratio for DMPC/DMPS/DMPE/Chol.

The setup consists of a screen-printed electrochemical sensor (BVT TECHNOLOGIES, BVT-AC1) with a silver reference electrode and gold counter- and working electrodes (1 mm diameter) which are mounted in a custom-made flow cell. Prior to every experiment, sensors were first immersed in a methanol bath and sonicated for 20 min to remove any organic residues. The sensor was then plasma-cleaned before mounting to the flow chamber. EIS spectra were measured using a PalmSens4 potentiostat (PalmSense BV, The Netherlands). The ac voltage was set to 10 mV (0 V dc offset), and the sensor's impedance was measured for frequencies between 1 mHz and 1 MHz subdivided into 30 logarithmically distributed data points. The liquid flow through the chamber was controlled using a computer-controlled syringe pump. Both the potentiostat as well as the syringe pump were controlled through MATLAB.

The real and imaginary parts of the recorded sensor impedance were fitted simultaneously to the Randles circuit (Figure 9)[49] using the impedance.py Python library (version 1.4.1).[50] The buffer is represented by a single resistor R_{sol} in series with a double-layer impedance which consists of a

https://doi.org/10.1021/acsinfecdis.2c00017
ACS Infect. Dis. 2022, 8, 2059−2072

parallel circuit of the double-layer capacitance C_m and double-layer resistance. The double-layer capacitance was modeled by a constant-phase element; the double-layer resistance is a series of a resistor R_m with a Warburg element W_m.

The Randles circuit was found to model signals from a membrane-coated and noncoated sensor; however, we note that the interpretation of the double-layer term varies for both systems. In the absence of any coating, the double-layer impedance originates from the formation of the Gouy−Chapman layer at the surface of the sensor.[51] In contrast, when coated with a membrane, the double-layer term corresponds to the membrane's electrical properties and the Gouy−Chapman layer can be neglected as it has been suggested previously.[52]

A sequence of three buffers was successively pumped into the chamber: (1) buffer A: potassium hexacyanoferrate(III) ($K_3[Fe(CN)_6]$) at a concentration of 5 mM. (2) Buffer B: vesicles formed from the cholesterol-depleted renal membrane analogue in 5 mM potassium hexacyanoferrate(III) ($K_3[Fe(CN)_6]$). (3) Buffer C: A sample buffer consisting of either 25 μg/mL PmB, 25 μg/mL of PmB in the erythro-PmBs, or 4.5 mg/mL of erythrocyte liposomes in 5 mM potassium hexacyanoferrate(III) ($K_3[Fe(CN)_6]$). In the first step, the flow chamber is flushed with *Buffer A*. Ten EIS spectra are recorded in time intervals of ≈1 min. Afterward, *Buffer B* is pumped into the chamber. EIS spectra are monitored for 90 min in time intervals of ≈1 min. Finally, *Buffer C* is pumped into the chamber. EIS spectra are recorded immediately after every movement of the syringe pump.

MD Simulations. Atomistic membrane simulations were conducted with GROMACS 5.1.4 on a GPU-accelerated computer workstation equipped with a 40-core central processing unit (CPU, Intel(R) Xeon(R) CPU E5-2630 v4 2.20 GHz), 130 GB random-access memory (RAM), and three graphic processing units (GPU, 2 NVIDIA 1080 TDI +1 GeForce GT 730). The simulations were set up using the CHARMM-GUI using the charmm36m force field.

Simulations were composed of ≈120 lipids in the upper and lower leaflet, respectively. The lipid composition of the pure erythrocyte membrane was based on previous lipidomics measured as detailed in ref 53. In brief, the major lipids composing the upper leaflet were SAPA (14.6 mol %), PLPC (7.2 mol %), POPC (4.7 mol %), PLA2 (3.2 mol %), POPE (3.1 mol %), SDPS (2.2 mol %), and SLPS (2.1 mol %). Other lipids found in smaller amounts were SLPC, PLA2, SAPE, PLPE, DPPC, and SOPE. Both the upper and lower leaflet contained 40 mol % cholesterol. The lower leaflet consisted of the following major lipids: PSM (15.4 mol %), PLPC (13.7 mol %), CER241 (11.84 mol %), LSM (9.3 mol %), POPC (6.4 mol %), SLPC (4.4 mol %), PAPC (3.6 mol %), CER220 (3.5 mol %), and CER3E (1.9 mol %). Lipid compositions were then further adjusted to account for hybrid erythrocyte membranes containing 5 and 10 mol % DMPS, respectively.

All systems were first energy-minimized and then equilibrated using an NVT/NPT ensemble before being simulated for 250 ns. All simulations used a 2 fs time step, a periodic boundary condition was applied to all directions, the particle-mesh Ewald to solve for long-range electrostatics, a short-range van der Waals cutoff of 1.2 nm, and the LINCS algorithm to determine bond constraints.[54,55] Temperature and pressure were maintained at 303 K and 1.0 bar, respectively, using a Nose−Hoover thermostat at 30 °C (τ = 0.5 ps) and Parrinello−Rahman semi-isotropic weak coupling (τ = 1 ps).[56,57] Simulations were analyzed and visualized using the Visual Molecular Dynamics software package (VMD).[58]

AUTHOR INFORMATION

Corresponding Author

Maikel C. Rheinstädter − *Department of Physics and Astronomy and Origins Institute, McMaster University, Hamilton L8S 4M1 Ontario, Canada;* orcid.org/0000-0002-0558-7475; Phone: +1-(905)-525-9140-23134; Email: rheinstadter@mcmaster.ca; Fax: +1-(905)-546-1252

Authors

Hannah Krivić − *Department of Physics and Astronomy and Origins Institute, McMaster University, Hamilton L8S 4M1 Ontario, Canada*

Sebastian Himbert − *Department of Physics and Astronomy and Origins Institute, McMaster University, Hamilton L8S 4M1 Ontario, Canada*

Ruthie Sun − *Department of Physics and Astronomy and Origins Institute, McMaster University, Hamilton L8S 4M1 Ontario, Canada*

Michal Feigis − *Department of Physics and Astronomy and Origins Institute, McMaster University, Hamilton L8S 4M1 Ontario, Canada*

Complete contact information is available at: https://pubs.acs.org/10.1021/acsinfecdis.2c00017

Notes

The authors declare no competing financial interest.

ACKNOWLEDGMENTS

This research was funded by the Natural Sciences and Engineering Research Council of Canada (NSERC), the Canada Foundation for Innovation (CFI), and the Ontario Ministry of Economic Development and Innovation. H.K is the recipient of a Canada Graduate Scholarship-Master's (CGS-M). S.H. is a Thode fellow of McMaster. M.C.R. is the recipient of an Early Researcher Award from the Province of Ontario and a University Scholar of McMaster University. The funders had no role in study design, data collection, analysis, decision to publish, or preparation of the manuscript.

REFERENCES

(1) Wright, G. D. *Curr. Opin. Microbiol.* **2010**, *13*, 589−594.
(2) Laxminarayan, R.; et al. *Lancet Infect. Dis.* **2013**, *13*, 1057−1098.
(3) Ventola, C. L. *Pharm. Ther.* **2015**, *40*, 277.
(4) Ventola, C. L. *Pharm. Ther.* **2015**, *40*, 344.
(5) Khondker, A.; Rheinstädter, M. C. *Commun. Biol.* **2020**, *3*, 77.
(6) Paterson, D. L. *Am. J. Infect. Control* **2006**, *34*, S20−S28.
(7) Brown, E. D.; Wright, G. D. *Nature* **2016**, *529*, 336−343.
(8) Yuan, Z.; Tam, V. H. *Expert Opin. Invest. Drugs* **2008**, *17*, 661−668.
(9) Zavascki, A. P.; Goldani, L. Z.; Li, J.; Nation, R. L. *J. Antimicrob. Chemother.* **2007**, *60*, 1206−1215.
(10) Khondker, A.; Dhaliwal, A. K.; Saem, S.; Mahmood, A.; Fradin, C.; Moran-Mirabal, J.; Rheinstädter, M. C. *Commun. Biol.* **2019**, *2*, 67.
(11) Trimble, M. J.; Mlynárčik, P.; Kolář, M.; Hancock, R. E. *Cold Spring Harbor Perspect. Med.* **2016**, *6*, a025288.
(12) Azad, M. A.; Finnin, B. A.; Poudyal, A.; Davis, K.; Li, J.; Hill, P. A.; Nation, R. L.; Velkov, T.; Li, J. *Antimicrob. Agents Chemother.* **2013**, *57*, 4329−4335.
(13) Khondker, A.; Alsop, R. J.; Dhaliwal, A.; Saem, S.; Moran-Mirabal, J. M.; Rheinstädter, M. C. *Biophys. J.* **2017**, *113*, 2016−2028.

(14) Abdelraouf, K.; Braggs, K. H.; Yin, T.; Truong, L. D.; Hu, M.; Tam, V. H. *Antimicrob. Agents Chemother.* **2012**, *56*, 4625−4629.
(15) Sandri, A. M.; et al. *Clin. Infect. Dis.* **2013**, *57*, 524−531.
(16) Zavascki, A. P.; Nation, R. L. *Antimicrob. Agents Chemother.* **2017**, *61*, No. e02319.
(17) Kalhapure, R. S.; Suleman, N.; Mocktar, C.; Seedat, N.; Govender, T. *J. Pharm. Sci.* **2015**, *104*, 872−905.
(18) Baptista, P. V.; McCusker, M. P.; Carvalho, A.; Ferreira, D. A.; Mohan, N. M.; Martins, M.; Fernandes, A. R. *Front. Microbiol.* **2018**, *9*, 1441.
(19) Hemeg, H. A. *Int. J. Nanomed.* **2017**, *12*, 8211.
(20) Brown, A. N.; Smith, K.; Samuels, T. A.; Lu, J.; Obare, S. O.; Scott, M. E. *Appl. Environ. Microbiol.* **2012**, *78*, 2768−2774.
(21) Khondker, A.; Malenfant, D. J.; Dhaliwal, A. K.; Rheinstädter, M. C. *ACS Infect. Dis.* **2018**, *4*, 926−935.
(22) Shaker, M. A.; Shaaban, M. I. *Int. J. Pharm.* **2017**, *525*, 71−84.
(23) Alhajlan, M.; Alhariri, M.; Omri, A. *Antimicrob. Agents Chemother.* **2013**, *57*, 2694−2704.
(24) Drulis-Kawa, Z.; Dorotkiewicz-Jach, A. *Int. J. Pharm.* **2010**, *387*, 187−198.
(25) Pierigè, F.; Serafini, S.; Rossi, L.; Magnani, M. *Adv. Drug Delivery Rev.* **2008**, *60*, 286−295.
(26) Muzykantov, V. R. *Expert Opin. Drug Delivery* **2010**, *7*, 403−427.
(27) Villa, C. H.; Anselmo, A. C.; Mitragotri, S.; Muzykantov, V. *Adv. Drug Delivery Rev.* **2016**, *106*, 88−103.
(28) Zaitsev, S.; et al. *Blood* **2012**, *119*, 4779−4785.
(29) Lorentz, K. M.; Kontos, S.; Diaceri, G.; Henry, H.; Hubbell, J. A. *Sci. Adv.* **2015**, *1*, No. e1500112.
(30) Lowe, G.; et al. *J. Emerg. Nurs.* **2008**, *34*, 26−32.
(31) Márquez, M. G.; Favale, N. O.; Leocata Nieto, F. L.; Pescio, L. G.; Sterin-Speziale, N. *Biochim. Biophys. Acta, Biomembr.* **2012**, *1818*, 491−501.
(32) Solopova, A.; van Gestel, J.; Weissing, F. J.; Bachmann, H.; Teusink, B.; Kok, J.; Kuipers, O. P. *Proc. Natl. Acad. Sci.* **2014**, *111*, 7427−7432.
(33) Omri, A.; Suntres, Z. E.; Shek, P. N. *Biochem. Pharmacol.* **2002**, *64*, 1407−1413.
(34) Alipour, M.; Halwani, M.; Omri, A.; Suntres, Z. E. *Int. J. Pharm.* **2008**, *355*, 293−298.
(35) McAllister, S.; Alpar, H.; Brown, M. *J. Antimicrob. Chemother.* **1999**, *43*, 203−210.
(36) Le, H.; Arnoult, C.; Dé, E.; Schapman, D.; Galas, L.; Le Cerf, D.; Karakasyan, C. *Biomacromolecules* **2021**, *22*, 1639−1653.
(37) The United States Committee on Antimicrobial Susceptibility Testing (USCAST). 2021, [Version 7.0], http://www.uscast.org (accessed Jan 2, 2022).
(38) Gonzalez Gomez, A.; Hosseinidoust, Z. *ACS Infect. Dis.* **2020**, *6*, 896−908.
(39) Sachetelli, S.; Khalil, H.; Chen, T.; Beaulac, C.; Sénéchal, S.; Lagacé, J. *Biochim. Biophys. Acta, Biomembr.* **2000**, *1463*, 254−266.
(40) Foteini, P.; Pippa, N.; Naziris, N.; Demetzos, C. *J. Liposome Res.* **2019**, *29*, 313−321.
(41) Zahednezhad, F.; Saadat, M.; Valizadeh, H.; Zakeri-Milani, P.; Baradaran, B. *J. Controlled Release* **2019**, *305*, 194−209.
(42) Himbert, S.; et al. *PLoS One* **2022**, *17*, No. e0263671.
(43) Himbert, S.; Alsop, R. J.; Rose, M.; Hertz, L.; Dhaliwal, A.; Moran-Mirabal, J. M.; Verschoor, C. P.; Bowdish, D. M. E.; Kaestner, L.; Wagner, C.; Rheinstädter, M. C. *Sci. Rep.* **2017**, *7*, 39661.
(44) Himbert, S.; Blacker, M. J.; Kihm, A.; Pauli, Q.; Khondker, A.; Yang, K.; Sinjari, S.; Johnson, M.; Juhasz, J.; Wagner, C.; Stöver, M. C.; Rheinstädter, M. C. *Adv. Biosyst.* **2020**, *4*, 1900185.
(45) Veatch, S. L.; Keller, S. L. *Biochim. Biophys. Acta, Mol. Cell Res.* **2005**, *1746*, 172−185.
(46) Juhasz, J.; Sharom, F. J.; Davis, J. H. *Biochim. Biophys. Acta, Biomembr.* **2009**, *1788*, 2541−2552.
(47) Juhasz, J.; Davis, J. H.; Sharom, F. J. *Biochem. J.* **2010**, *430*, 415−423.
(48) Juhasz, J.; Sharom, F. J.; Davis, J. H. *Biochim. Biophys. Acta, Biomembr.* **2009**, *1788*, 2541−2552.
(49) Randles, J. E. B. *Discuss. Faraday Soc.* **1947**, *1*, 11−19.
(50) Murbach, M. D.; Gerwe, B.; Dawson-Elli, N.; Tsui, L.-k. *J. Open Source Software* **2020**, *5*, 2349.
(51) Oldham, K. B. *J. Electroanal. Chem.* **2008**, *613*, 131−138.
(52) Steinem, C.; Janshoff, A.; Ulrich, W.-P.; Sieber, M.; Galla, H.-J. *Biochim. Biophys. Acta, Biomembr.* **1996**, *1279*, 169−180.
(53) Himbert, S.; Qadri, S. M.; Sheffield, W. P.; Schubert, P.; D'Alessandro, A.; Rheinstädter, M. C. *PLoS One* **2021**, *16*, No. e0259267.
(54) Darden, T.; York, D.; Pedersen, L. *J. Chem. Phys.* **1993**, *98*, 10089−10092.
(55) Hess, B.; Bekker, H.; Berendsen, H.; Fraaije, J. *J. Comput. Chem.* **1997**, *18*, 1463−1472.
(56) Evans, D.; Holian, B. *J. Chem. Phys.* **1985**, *83*, 4069−4074.
(57) Parrinello, M.; Rahman, A. *J. Appl. Phys.* **1981**, *52*, 7182−7190.
(58) Humphrey, W.; Dalke, S.; Schulten, K. *J. Mol. Graphics* **1996**, *14*, 33−38.